



Linear and nonlinear optical characteristics of PVA/CMC/PEG blended polymer loaded with ZnS formed at different temperatures

A. M. El-naggar¹, Zein K. Heiba², A. M. Kamal³, Omar H. Abd-Elkader³, G. Lakshminarayana⁴, and Mohamed Bakr Mohamed^{2,*}

¹ Research Chair of Exploitation of Renewable Energy Applications in Saudi Arabia, Physics & Astronomy Department, College of Science, King Saud University, P.O. Box 2455, Riyadh 11451, Saudi Arabia

² Physics Department, Faculty of Science, Ain Shams University, Cairo, Egypt

³ Physics & Astronomy Department, College of Science, King Saud University, P.O. Box 2455, Riyadh 11451, Saudi Arabia

⁴ Intelligent Construction Automation Center, Kyungpook National University, 80 Daehak-Ro, Buk-Gu, Daegu 41566, Republic of Korea

Received: 25 July 2022

Accepted: 30 October 2022

Published online:

13 January 2023

© The Author(s), under exclusive licence to Springer Science+Business Media, LLC, part of Springer Nature 2023

ABSTRACT

Pure and loaded polyvinyl alcohol/carboxymethyl cellulose/polyethylene glycol (PVA/CMC/PEG: 70/15/15%) blends with zinc sulfide (ZnS) were prepared at different temperatures (200, 300, 400, and 500 °C) using solid state reaction at low temperatures and casting procedures. The phases formed, cell parameters, crystallite size, and lattice microstrain parameters of the nanofillers (ZnS at different temperatures) were investigated using the Rietveld method. The obtained polymer blends loaded with ZnS were characterized using X-ray diffraction, Fourier transform infrared, and scanning electron microscope techniques. The impact of loading ZnS on the linear and nonlinear optical parameters of the blended polymers was explored in detail. The optical energy (E_g) values (direct = 5.52 eV and indirect = 5.12 eV) of the PVA/CMC/PEG blend were decreased upon loading with ZnS, attaining the lowest values (3.56 and 3.11) eV with ZnS prepared at 300 °C. The refractive index of the pristine blend decreased monotonically with the wavelength, while for the loaded blend, it decreased with (λ) up to 320 nm, then increased in the range $350 \leq \lambda \leq 450$ nm, then decreased slowly. The NLO parameters attained their maximum values in the visible range as the blend was loaded with ZnS and prepared at 300 °C. The fluorescence emitted colors and intensities of the blended polymer depended on the prepared temperature of the nanofiller.

Address correspondence to E-mail: mbm1977@yahoo.com

1 Introduction

Blended polymers have recently received more attention than single polymers due to the former's novel properties [1–4]. Furthermore, polymer blending reveals a variety of appealing properties that are dependent on the miscibility and degree of compatibility interaction between the functional groups in pristine polymers [5]. Polyvinyl alcohol (PVA) polymer has several advantages, such as solubility in water, nontoxicity, biodegradability, and good optical performance [6]. Carboxymethyl cellulose (CMC) is one of the cellulose derivative compounds that are used in several applications owing to their great properties. CMC has a semi-crystalline nature, and it exhibits non-toxicity, eco-friendliness, biocompatibility, water-solubility, and biodegradability [7]. Polyethylene glycol (PEG) has significant characteristics such as superb water solubility, good protein adsorption resistance, low toxicity, and poor immunogenicity. The optical features of PVA were improved as it blended with PEG, where the optical band gap of PVA was decreased while Urbach energy and refractive index were increased as the content of PEG increased in the PVA/PEG blend [8].

Moreover, the characteristics of a polymer or blended polymer can be tuned as they are doped with suitable compounds [7]. The linear and nonlinear optical characteristics of a polymer or blended polymer can be tuned as they are doped with nano semiconductor materials [9]. Doping the PVA/CMC blend with different crystallite sizes of nano gold (using the pulsed laser ablation technique) affected its optical and electric characteristics [2]. The optical parameters of polyvinyl pyrrolidone and polyethylene oxide were improved as a result of the inclusion of copper oxide nanoparticles [10]. The positive nonlinear absorption coefficient and negative nonlinear refraction indices indicate that ZnSe/PVA films are appropriate materials in nonlinear optical applications [11]. When PVA/PEG was doped with Ag_2S , a high value of third-order susceptibility was discovered [12]. The optical absorbance spectra obtained from the CdS/PVA films can be utilized for a favorable optical bandgap that could be employed in solar cell window layer applications [13].

Zinc sulfide (ZnS) is one of the wide band gap semiconductor materials that has several structures based on the conditions of production. Furthermore, the performance of ZnS can be controlled as its size

changes using different preparation methods at different annealing temperatures. Tiwari et al. found the stabilization of ZnS nanoparticles by polymeric matrices. As a result, it has the potential to be used in a variety of fields, including biosensing, cell tagging, optoelectronic devices, heterogeneous catalysis, photocatalytic application, drug delivery, labeling, tracking agents, bioanalytical sensors, fluorescent probes, optics, information storage, and optoelectronics [14]. Furthermore, Pizarro et al. designed a photo-switchable polymeric system in the presence of nano ZnS under the influence of UV Light irradiation [15].

The linear optical properties varied with the incorporation of CdS NPs with different crystallite sizes within PVA. The PVA film with CdS nucleated at 200 °C was found to be appropriate for bio-related purposes like bio-labeling, bio-imaging, drug delivery, and LEDs as well as a window layer in solar cells [16].

In this work, the high optical band gap value of the pure blend (> 5 eV) indicated the good absorbance of the blend in the UV range, which represented about 9% of the total solar power received at the surface of the earth. The reduction of the optical band gap of the blend upon loading with different crystallite sizes of the nanofiller allowed it to absorb more energy from the solar radiation from other wavelength ranges. Therefore, ZnS NPs with different crystallite sizes were fabricated using the solid state reaction method at low temperature and combined with PVA/CMC/PEG. The structures and linear and nonlinear optical characteristics of the prepared blends, along with their possible applications, were examined in detail.

2 Materials and methods

Zinc sulfide samples (ZnS) were produced at different temperatures (200, 300, 400 and 500 °C) using a solid-state procedure. The samples were produced by mixing, grinding, and heating zinc acetate dihydrate and thiourea at different temperatures: 200, 300, 400, and 500 °C (3 h), separately. The pure and loaded PVA/CMC/PEG (70/15/15%) blends with ZnS prepared at different temperatures were prepared using a casting procedure by dissolving 0.7 g of polyvinyl alcohol (PVA) (molecular weight = 50,000 g/mol), 0.15 g carboxymethyl cellulose (CMC) (in the form of the sodium salt of commercial grade), and

0.15 g of polyethylene glycol (PEG, MW = 4000 g/mol) in 70, 15 and 15 ml of distilled water in the presence of the nanofillers and following the same steps as in Ref. [7, 17, 18]. The obtained blends have a thickness of 160–210 μm (measured by a digital micrometer with accuracy and ± 1 μm).

The nanofillers and blended polymers were characterized by X-ray diffraction (PANalytical diffractometer, X'pert MPD, Philips, λ = 1.5418 Å). A JASCO-V-670 spectrophotometer with an attached integrating sphere assembly technique was used to measure the diffused absorbance and reflectance spectra for each sample. A FP-8200 JASCO luminescence spectrophotometer was used to investigate the emission spectra of the blended polymer films. Fourier transform infrared (FTIR) spectroscopy (Bruker Tensor 27 FTIR Spectrometer) and scanning electron microscopy (JEOL, Akishima, Tokyo, Japan, JED- 2200 Series) were employed to investigate the morphology, compositions, and structures of the different blends.

The refractive index (n) and extinction coefficient (k) of the different polymers were estimated by [17, 18]:

$$n = \frac{1 + R}{1 - R} + \sqrt{\frac{4R}{(R - 1)^2} - k^2} \tag{1}$$

$$k = \frac{\lambda\alpha}{4\pi} \tag{2}$$

$$\alpha(\lambda) = \left(\frac{2.303}{d}\right)A \tag{3}$$

where R, α, λ, A, and d are reflectance, absorption coefficient, wavelength, absorbance, and thickness of the film, respectively.

The real (ε_r) and imaginary (ε_i) dielectric constant parts, the optical conductivity (σ_{opt}), surface energy loss function (SELF), volume energy loss function (VELF), linear optical susceptibility, χ⁽¹⁾, third-order nonlinear optical susceptibility (χ⁽³⁾), and nonlinear refractive index (n₂) of all films were obtained using [17, 18]:

$$\epsilon_r = n^2 - k^2 \tag{4}$$

$$\epsilon_i = 2nk \tag{5}$$

$$\sigma_{opt} = \frac{\alpha n C}{4\pi} \tag{6}$$

$$SELF = \frac{\epsilon_i}{(\epsilon_r + 1)^2 + \epsilon_i^2} \tag{7}$$

$$VELF = \frac{\epsilon_i}{\epsilon_r^2 + \epsilon_i^2} \tag{8}$$

$$\chi^{(1)} = \frac{1}{4\pi} (n^2 - 1) \tag{9}$$

$$\chi^{(3)} = 1.7 \times 10^{-10} \left(\chi^{(1)}\right)^4 = 1.7 \times 10^{-10} \left(\frac{n^2 - 1}{4\pi}\right)^4 \tag{10}$$

$$n_2 = \frac{12\pi}{n} \chi^{(3)} \tag{11}$$

where C, k_B, and T are the velocity of the light, the Boltzmann constant, and the temperature in Kelvin, respectively.

3 Results and discussion

3.1 Structural and morphology evaluations

Phase analysis of the obtained x-ray diffractograms manifested a single phase of cubic zincblende structure (F4̄3m) for all ZnS samples prepared at 200, 300, 400, and 500 °C. Applying the Rietveld method, the cell parameter, crystallite size, and lattice microstrain parameters have been determined for the samples, Table 1. Figure 1c and d illustrates the fitting between the measured and Rietveld-calculated diffraction patterns for T = 200 and 400 °C. A clear reduction in the peak-broadening could be noticed, indicating the increase in the crystallite size. Also, the peak intensities increased, indicating better crystallization, more lattice ordering, and a reduction in the number of defects. All samples exhibited an anisotropic crystallite size and microstrain. As expected, the size increased upon raising the annealing temperature and the microstrain was reduced, which could be

Table 1 Lattice parameter (a), crystallite size, and strain of ZnS prepared at different temperatures

T (°C)	a (Å)	Size (Å)		Strain	
		h00	hkh	h00	hkh
200	5.378(2)	17	26	0.0104	0.0109
300	5.396	33	41	0.0023	0.0023
400	5.409	36	63	0.0003	0.0002
500	5.395	43	40	0.0020	0.001

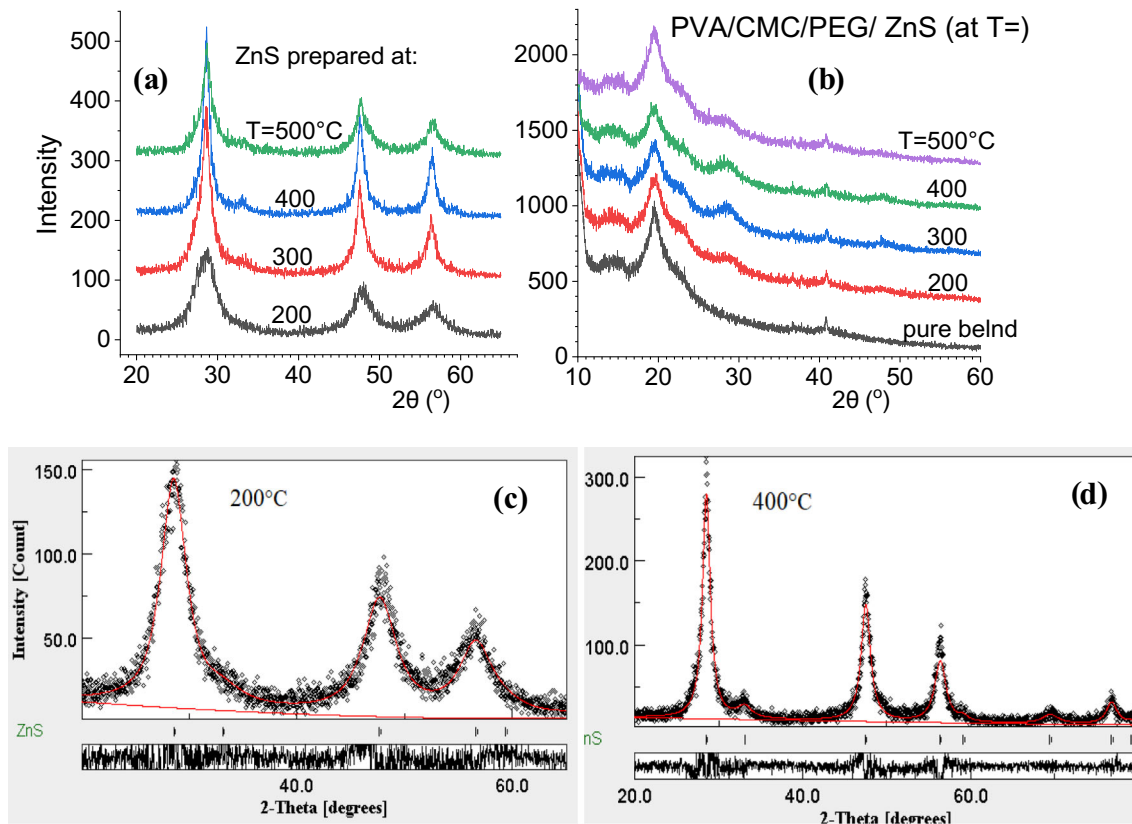


Fig. 1 X-ray diffraction spectra for **a** ZnS prepared at different temperatures, **b** PVA/CMC/PEG blended polymers loaded with ZnS prepared at different temperatures, and Rietveld refinement for ZnS prepared at **c** 200 and **d** 400 °C

attributed to the reduction in the quantity of defects. The cell parameter increased upon raising the temperature, which may be related to relieving the compressive strain by annealing. Similar behavior for ZnS was obtained by chemical precipitation [19], and it is attributed to the incorporation of O interstitially and the formation of ZnO.

The diffraction patterns for the blended polymers PVA/CMC/PEG (70:15:15) pure and doped with ZnS samples prepared at 200, 300, 400, and 500 °C as nanofiller are shown in Fig. 1b. The ZnS nanofiller exhibited no diffraction peaks due to its small percentage in the polymer blend. All patterns manifested a small degree of crystallinity with a high background due to the diffuse scattering. The diffraction patterns contain a main broad peak around $2\theta = 20^\circ$ and two wide humps around $2\theta = 14^\circ$ and 23° . A distinctive small peak is detected at around $2\theta = 41.5^\circ$. The non-crystalline polymer CMC is known to exhibit a diffraction hump around 20° [20, 21], and all other peaks arise from the

semicrystalline polymer PEG at $2\theta \sim 19.3^\circ$ and 23.5° [22, 23] and PVA at $2\theta \sim 19.2^\circ$ and 20.2° [24, 25].

SEM images were taken to follow the changes in the surface morphology of blended films. The effect of the annealing temperature of the nanofiller ZnS on the morphology of the PVA/CMC/PEG polymer blend is obvious as shown in Fig. 2a–e for pure and polymer blends loaded with ZnS prepared at 200, 300, 400, and 500 °C. A smooth surface with small pores nearly uniformly distributed is obtained for the pure polymer blend. The depth of pores and their size are increased upon loading with ZnS, Fig. 2b–e. As the annealing temperature of ZnS is raised, its particle size gets bigger (Table 1), which obviously affects the surface morphology of the blended film. The surface roughness clearly increased with increasing the pores. Figure 2e shows a heterogeneous surface with a larger pore size, cavity, and predominates for the blend loaded with ZnS at 500 °C. The EDS analysis for a polymer blend loaded with ZnS (400 °C) is given in Fig. 2f. The atomic percent of Zn ions (6.13%) is higher than that of S ions

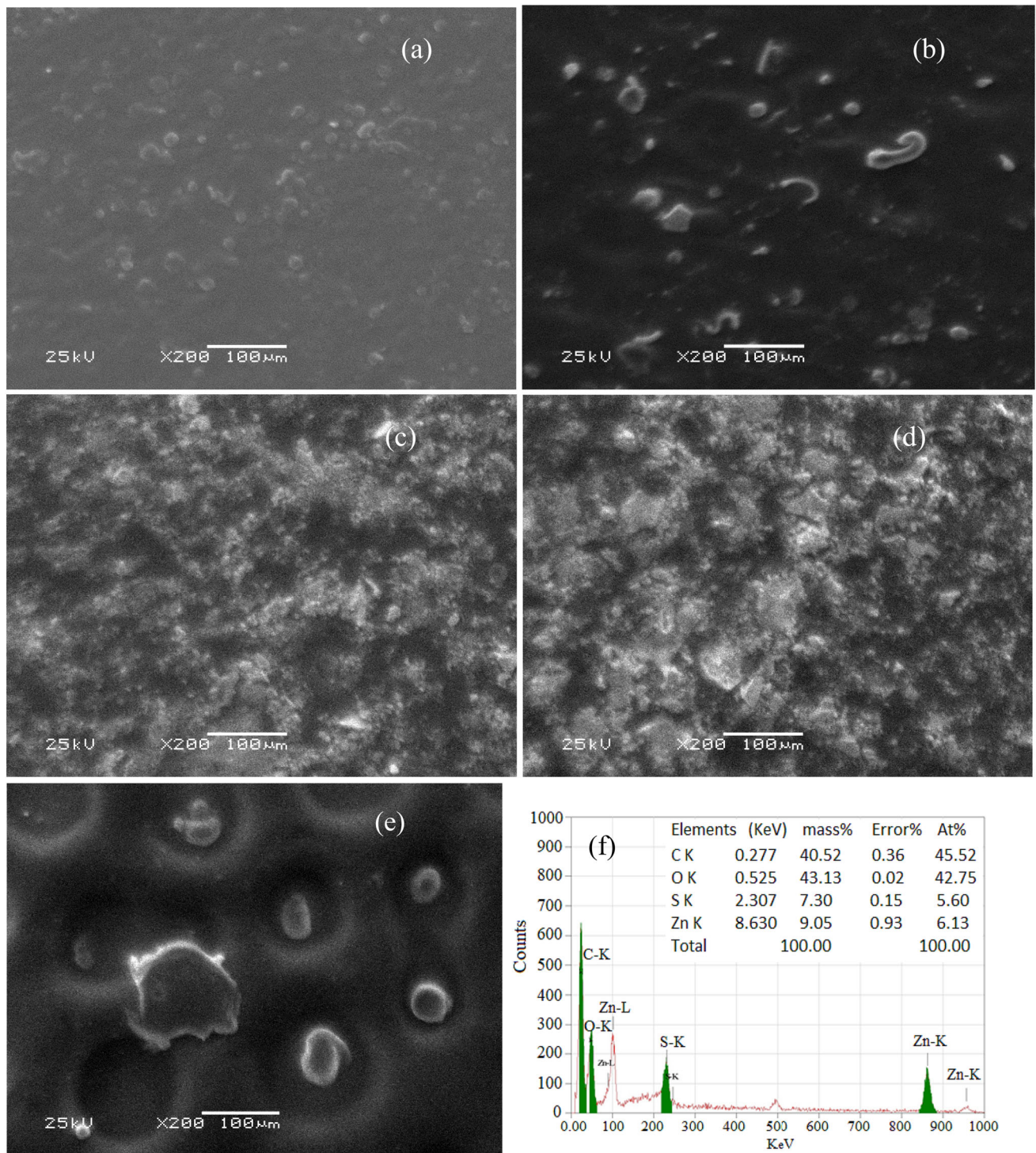


Fig. 2 a–e SEM images for PVA/CMC/PEG blended polymers loaded with ZnS prepared at different temperatures and f EDS for the blended polymer loaded with ZnS prepared at 400 °C

(5.6%), implying that some S ions have been replaced by O ions during the annealing of ZnS at 400 °C. The determined atomic percentages of the constituting elements are fairly close to the nominated values.

3.2 FT-IR transmission analysis

Figure 3 shows the FT-IR transmission measurements for the PVA/CMC/PEG blended polymers loaded with ZnS prepared at different temperatures.

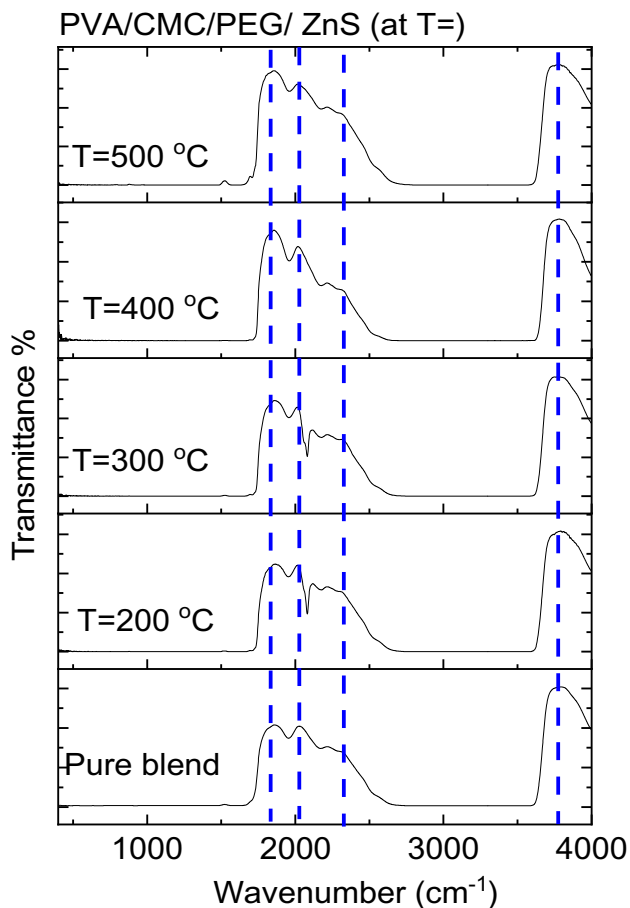


Fig. 3 FTIR spectra for PVA/CMC/PEG blended polymers loaded with ZnS prepared at different temperatures

Small variations in the location and intensities of the vibrational bands are observed in the vibrational bands associated with the loaded pure blend with the nanofillers. These changes are attributed to the replacement of some carbon and nitrogen atoms with ZnS prepared at different temperatures in the inner structure of the PVA/CMC/PEG blend. By inspecting the FTIR spectra for all blends, the OH stretching bond was detected at 3772 cm^{-1} [26], while $\text{C}\equiv\text{C}$, $\text{C}\equiv\text{N}$ and $\text{C}=\text{O}$ bonds are defined at 2308 , 2009 , and 1827 cm^{-1} , respectively [27, 28].

3.3 UV–vis spectroscopy investigations

Figure 4 reveals the absorbance (A), the transmittance (T), and the reflectance (R) spectra of the PVA/CMC/PEG/ZnS (at $T = 200, 300, 400$, and $500\text{ }^{\circ}\text{C}$) blended polymers. As the blend loaded with ZnS is prepared at different temperatures, the transmission is reduced, while both absorbance and reflectance are

increased. The bands detected at around 282 and 315 nm are defined as $\pi-\pi^*$ and $n-\pi^*$ transitions, respectively [29]. The absorption edge of the transmittance data exhibited a redshift towards the higher wavelength range due to the variation in the crystallite size of the nanofiller [6]. A similar result was observed as PVA or PVA/PVP loaded with different amounts of BaTiO_3 or (Gd_2O_3 or MgO) [1, 2, 6]. Also, a similar result was found as PVA/CMC doped with different amounts of SrTiO_3 [3]. The redshift in the transmittance indicated a variation in the band structure of the blended polymer as it was loaded with different nanofiller. The maximum redshift was raised as the blend loaded with ZnS prepared at $400\text{ }^{\circ}\text{C}$. In the visible range ($400 - 800\text{ nm}$), the transmittance spectra of all blends were nearly constant as the wavelength increased owing to the normal dispersion of light [6]. Furthermore, the blend loaded with ZnS has good absorbance performance for the UV spectra at $315\text{--}400\text{ nm}$ (UVA) and $280\text{--}315\text{ nm}$ (UVB) relative to the pure blend. The blends loaded with ZnS prepared at $[200, 300]$ and $[300, 400]\text{ }^{\circ}\text{C}$ have a maximum shielding for UVB and UVA types, respectively [30]. The changes in the reflectance spectra upon loading the blended polymers with different crystallite sizes of ZnS (Table 1) may be caused by the modifications in the packing density of the host blend [31]. A similar result was detected as a CMC/PVA blend loaded with nano NiO [4].

One of the most significant optical characteristics of a material is its direct and indirect (allowed and forbidden) optical band gaps, which are defined as the energy needed for the electron to hop between HOMO (highest-occupied molecular orbital) and LUMO (lowest unoccupied molecular orbital) [32].

The values of optical energy gap (E_g) were obtained using the following relation [11]:

$$h\nu = B(h\nu - E_g)^m \quad (12)$$

where h , ν and B are Planck's constant, frequency of the incident light, and a constant, respectively.

In order to determine the optical band gaps of different blends, plotting relations between $(\alpha h\nu)^{1/m}$ and $h\nu$ were formed, Fig. 5. The linear part is extrapolated to find the intercept on the $h\nu$ axis, which gives direct and indirect optical band gaps (E_g), Fig. 5a, b, respectively. The direct and indirect optical energy gaps for the PVA/CMC/PEG blend are 5.52 and 5.12 eV , respectively. The direct band

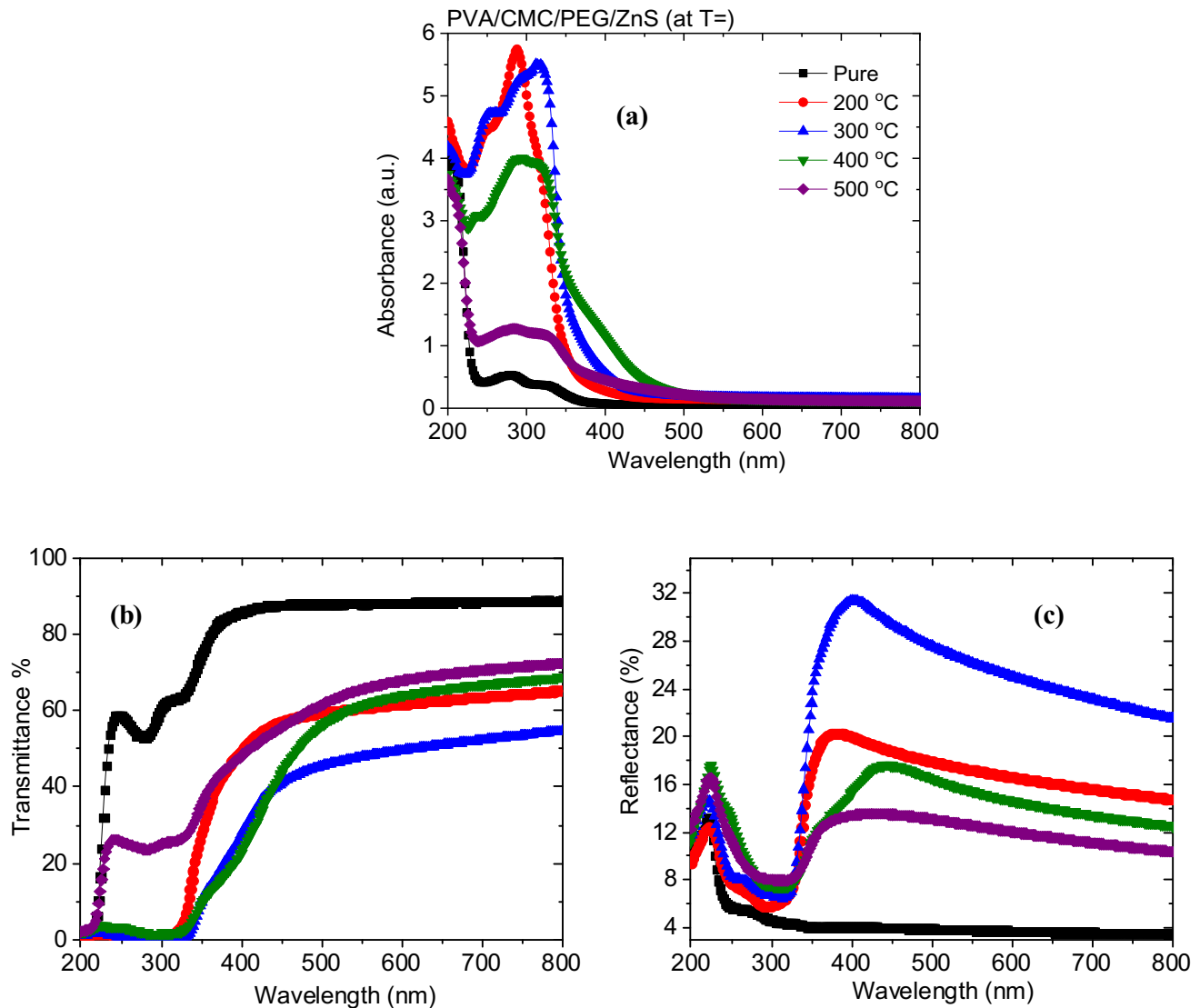


Fig. 4 a Absorbance, b transmittance, and c reflectance spectra for PVA/CMC/PEG blended polymers loaded with ZnS prepared at different temperatures

gap was decreased to (4.89, 3.69), (4.98, 3.56), (5.12, 3.42), and 5.41 eV. Furthermore, the indirect band gap also decreased to 3.31, 3.11, (3.40, 2.83) and 4.87 eV as the blend loaded with ZnS prepared at 200, 300, 400, and 500 °C, respectively. As revealed from the obtained results, E_g values of the PVA/CMC/PEG blend were reduced relative to the pure blend as it was loaded with ZnS prepared at different temperatures, and it reached its lowest values with ZnS prepared at 300 °C. This can be attributed to the increase in the degree of disordering within the band gap owing to the strong interaction that occurred between ZnS nanoparticles and the host blend matrix. This interaction was responsible for proper

changes in the optical band gap structure, increasing the number of defects and consequently forming unstructured localized states through which electrons can move more easily between HOMO and LUMO. The irregular changes in the optical band gaps of the loaded blends may be due to the variation in the internal structure of the host polymer besides the creation of a localized state inside the optical gap upon loading with ZnS [33]. Similar results were noticed as the PVA/PVP blend was loaded with Gd_2O_3 or MgO, respectively [1, 2, 32]. The direct and indirect E_g values of the PVA/CMC blend were reduced from 4 to 2.18 eV and from 4.84 to 2.96 eV as it was loaded with nano Se [6].

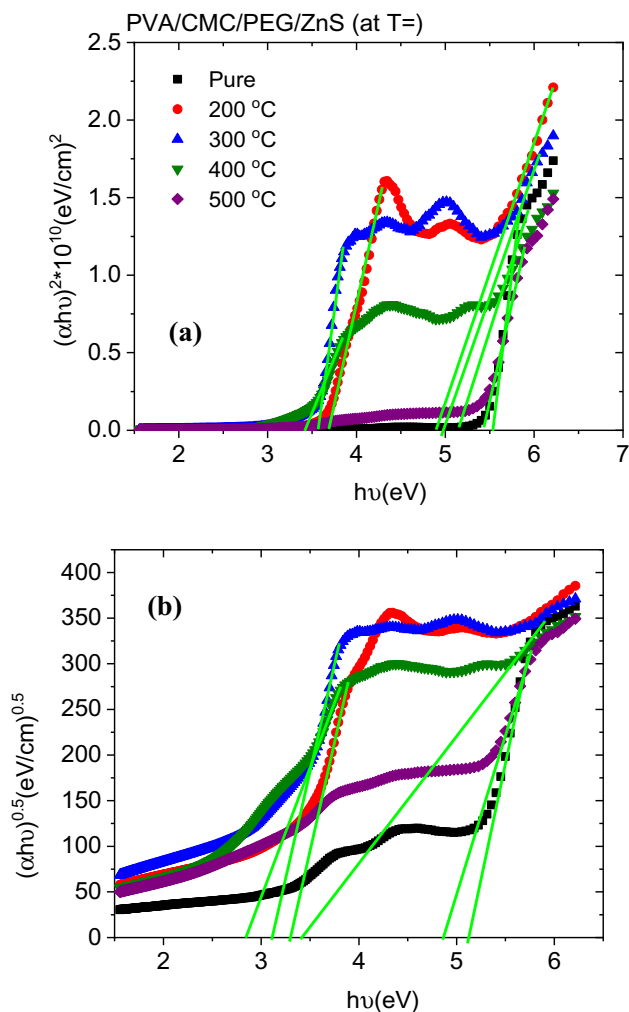


Fig. 5 **a** Direct and **b** indirect optical band gaps using Tauc's relation for PVA/CMC/PEG blended polymers loaded with ZnS prepared at different temperatures

The high optical band gap value of the pure blend ($> 5 \text{ eV}$) indicated the good absorbance of the blend in the UV range, which represented about 9% of total solar power received at the surface of the earth. The reduction of the optical band gap of the blend upon loading with different crystallite sizes of the nanofiller allowed it to absorb more energy from the solar radiation of the other wavelength ranges. Therefore, the resulting blends can be employed in many optoelectronic applications [34].

Figure 6 displays the variation of refractive index (n) and extinction coefficient (k) with the wavelength for pure and loaded PVA/CMC/PEG blends with ZnS prepared at different temperatures. In general, the k values for all blends were reduced as the wavelength increased in the wavelength range

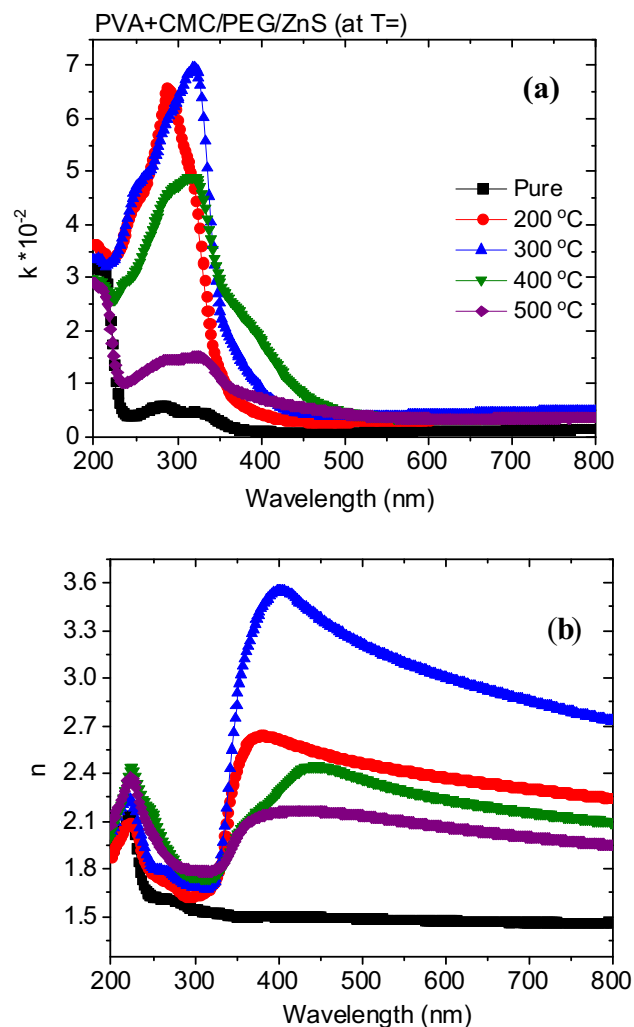


Fig. 6 Wavelength dependence of **a** the extinction coefficient and **b** the refractive index for PVA/CMC/PEG blended polymers loaded with ZnS prepared at different temperatures

between 210–400 nm, and the k value of loaded blends increased. The values of k for the PVA/CMC/PEG blend were increased as the blend was loaded with ZnS. In the UV range, blends with ZnS prepared at 200 and 300 °C have the maximum k values, while in the visible region, the blend with ZnS prepared at 400 °C has the highest value. This variation in the k value may be correlated to the absorption trend of the blends upon loading with different nanocrystal fillers and, consequently, a change in the interaction between the incident light and the free carriers present in the loaded blends with different crystal sizes of nanofiller [35].

In addition, as revealed from Fig. 6b, the n value of all blends was improved as the wavelength increased up to 230 nm, after that, it was reduced as the

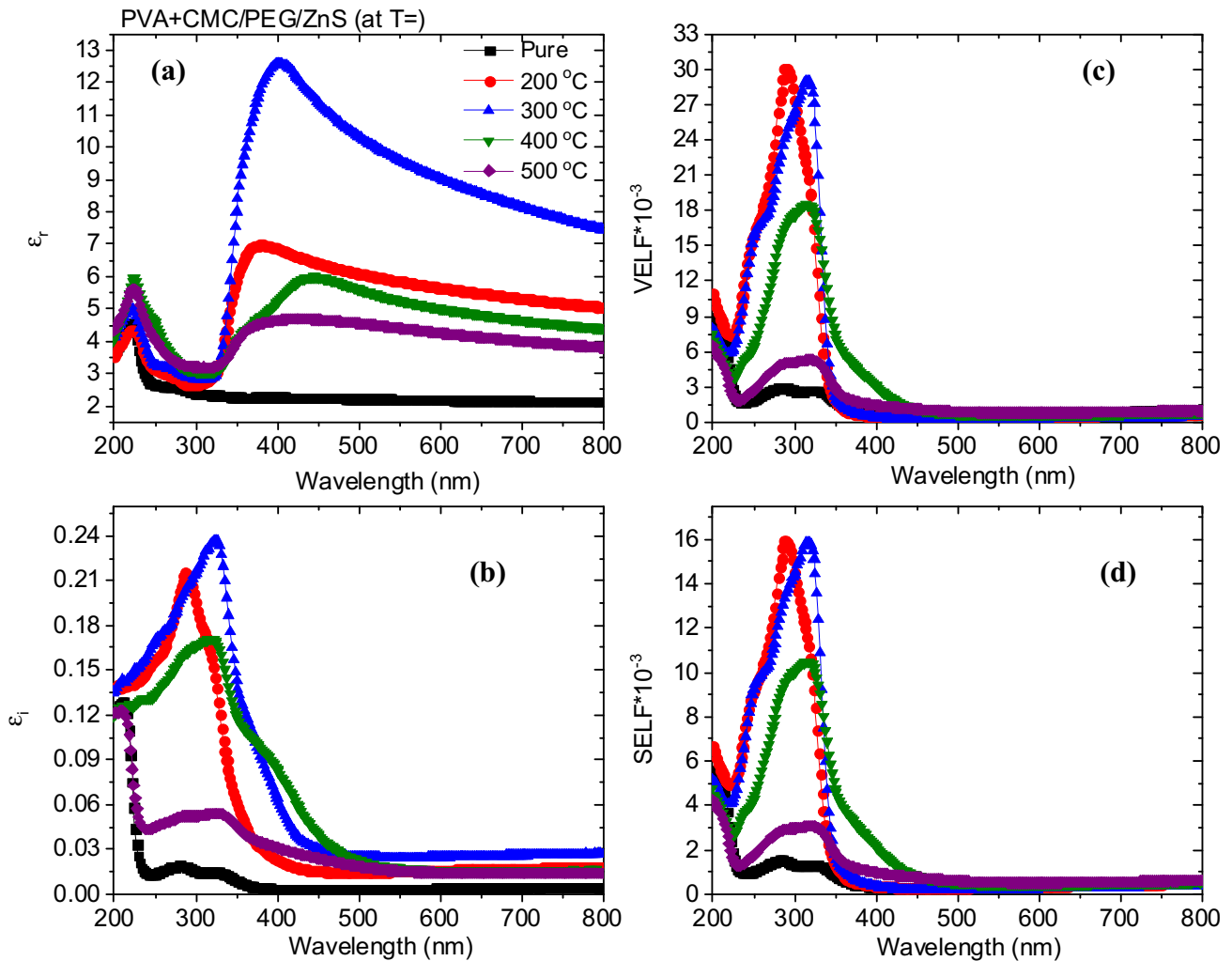


Fig. 7 a the real and b imaginary dielectric constant, c SELF, and d VELF for PVA/CMC/PEG blended polymers loaded with ZnS prepared at different temperatures

wavelength increased, except for the doped blends in λ range between 330–420 nm; the n values enlarged. Furthermore, the n value of the PVA/CMC/PEG blend was increased as the blend was loaded with ZnS. The n values attained their highest values in the UV range as the blend loaded with ZnS prepared at 400 °C, while in the visible range; the blend loaded with ZnS prepared at 300 °C has the highest values. The CMC/PVP blend exhibited a similar feature in the visible range [4]. This refractive index trend can be attributed to a change in the number of oscillating dipoles, which causes a redistribution of electronic charges and, as a result, a change in the polarizability of the blends [36]. As PVA/PVP is doped with Gd_2O_3 or MgO , the values of n change according to the amount of doping [1, 3]. The changes in the n values upon loading the blend with nanofiller may result

from the modification of the created intra-intermolecular bonding between nano ZnS and the blend matrix and hence the density of chain packing [37].

Figure 7a and b reveals the dependence of real (ϵ_r) and imaginary (ϵ_i) parts of the dielectric constant of the complex dielectric constant ϵ on the wavelength for all blends. Also, the surface and volume energy loss functions (SELF, VELF) are displayed too in Fig. 7c, d. For all the investigated blends, both ϵ_r and ϵ_i exhibited an exponential reduction in the visible range. Also, ϵ_r and ϵ_i have a similar trend, such as n and k , respectively. The values of ϵ_r and ϵ_i of the doped blends are higher than the pure blend. The blend loaded with ZnS prepared at 300 °C has the highest dielectric value. Furthermore, both SELF and VELF spectra exhibited similar performance. The value of VELF is larger than the corresponding SELF

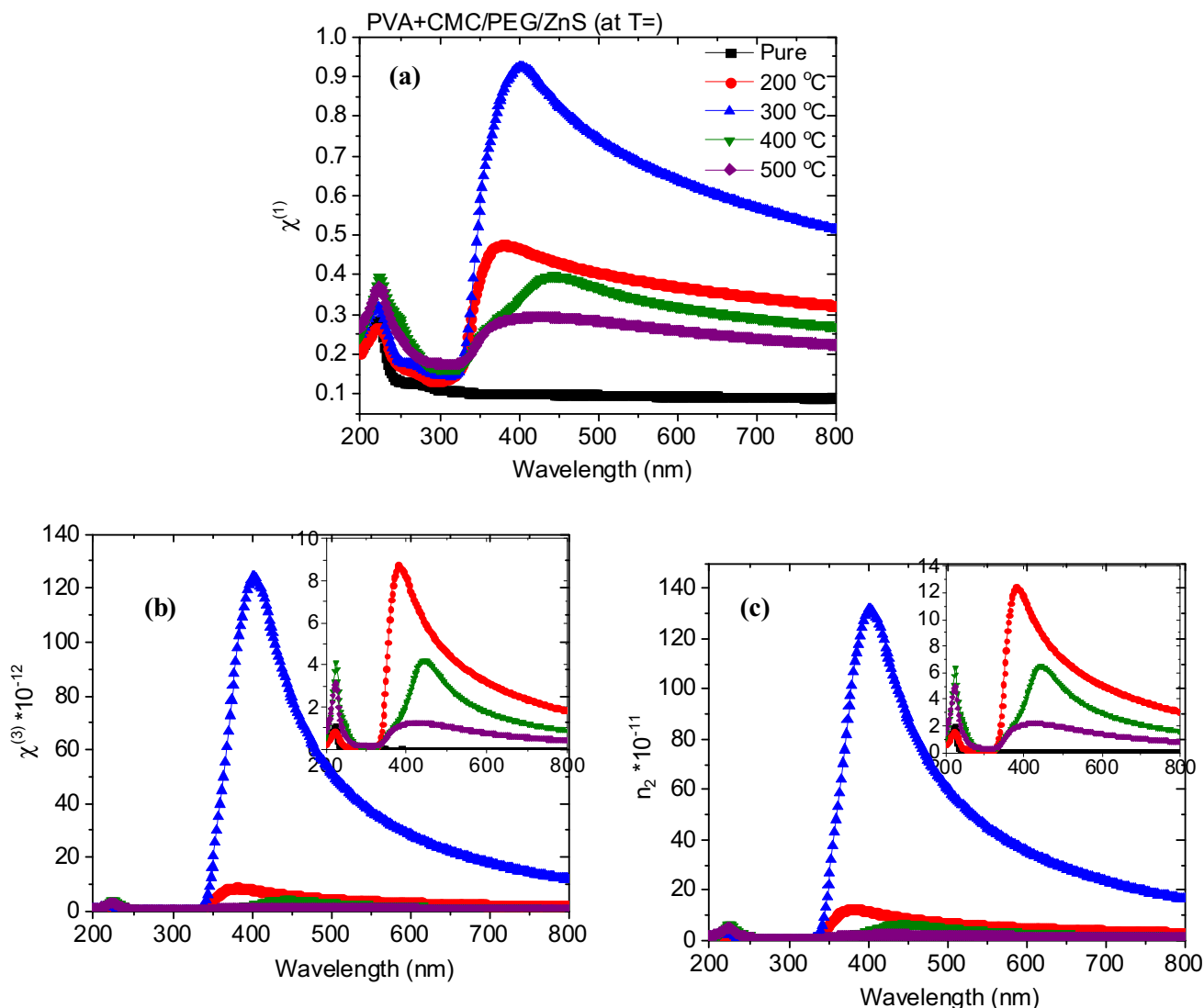


Fig. 8 The variations with wavelength for **a** linear optical susceptibility, **b** nonlinear third order, and **c** nonlinear refractive index for PVA/CMC/PEG blended polymers loaded with ZnS prepared at different temperatures

value. Both SELF and VELF in the loaded blends are higher than in the pure one. The blends with ZnS prepared at 200 and 300 °C have the greatest SELF and VELF values in the UV range, while in the visible range, the blend with ZnS prepared at 400 °C has the highest SELF and VELF values.

In addition, the first and third orders of optical susceptibility ($\chi^{(1)}$, $\chi^{(3)}$) and nonlinear refractive index (n_2) for all the blends are represented in Fig. 8. As seen from the graph, in the UV range, the nonlinear optical parameters ($\chi^{(1)}$, $\chi^{(3)}$ and $n_2 = \text{NLO}$) values first increased as the wavelength increased up to 320 nm, then reduced with a further increase in the wavelength values, except for the loaded blends in the wavelength range 320–400 nm, where the NLO

values were reduced. In addition, the values of NLO were increased as the blend was loaded with ZnS and attained their maximum value in the visible range as the blend was loaded with ZnS prepared at 300 °C. A similar result was obtained as a PVA/PVP blend loaded with Gd_2O_3 [1]. These large modifications in the values of NLO parameters in the visible range may result from the large refractive index n value of the loaded blend as compared with the pure blend in this range. The improvement of the NLO features of loaded blends upon being loaded with ZnS qualifies the produced blends to be employed in high-speed communications and fast optical switching applications.

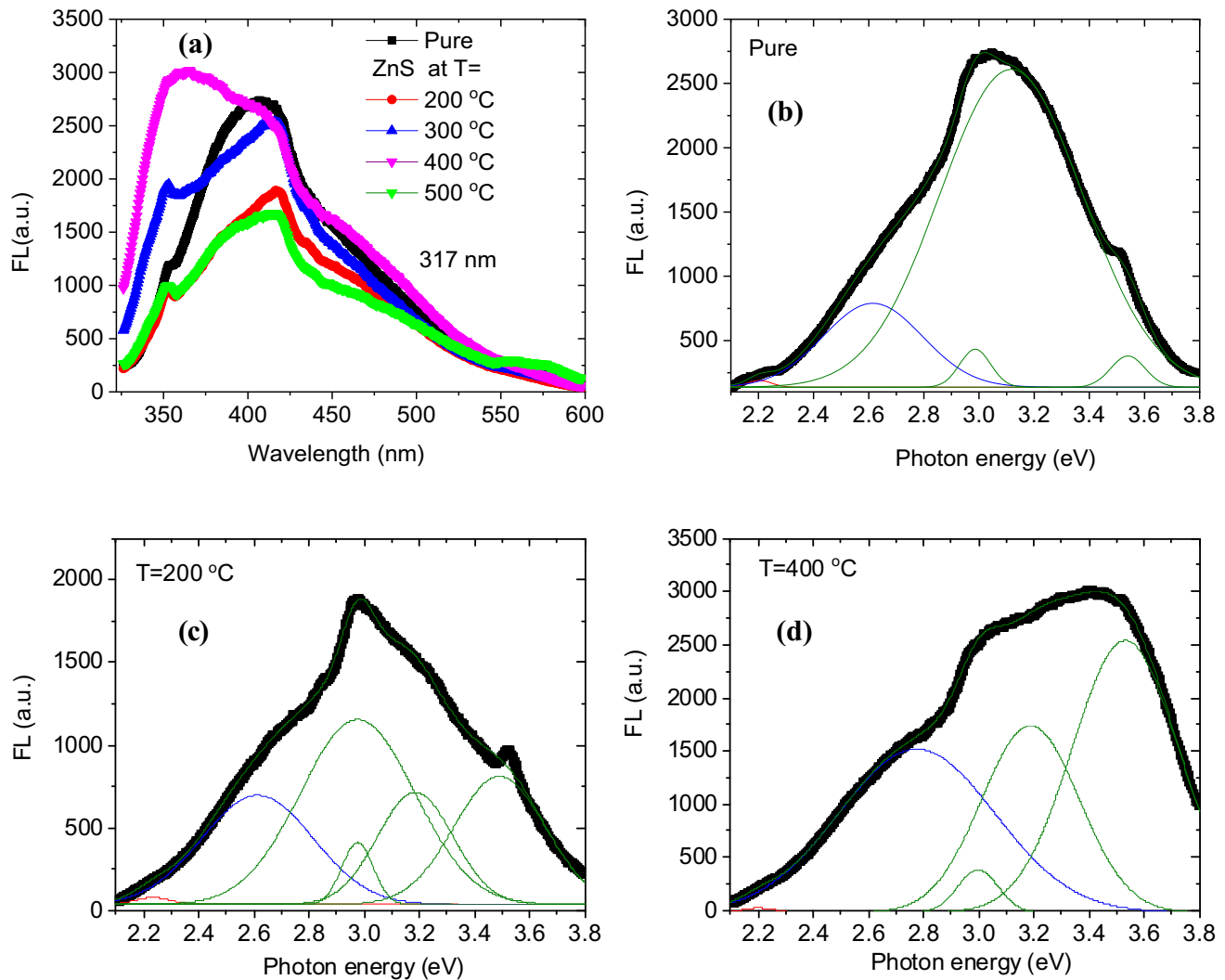


Fig. 9 a The FL spectra and b, c Gaussian fitting for PVA/CMC/PEG blended polymers loaded with ZnS prepared at different temperatures under excitation of 317 nm

3.4 Fluorescence (FL) characterization

Figure 9a illustrates the FL spectra of the PVA/CMC/PEG/ZnS nanocomposites excited at $\lambda = 317$ nm. A broad and asymmetric emission band can be seen between 320 and 500 nm, having a center that varies with the preparation temperature of the ZnS nanofiller. PVA displays a strong luminescence in the wavelength range $\lambda = 350$ –550 nm, which is assigned to the electronic transitions $\pi \rightarrow \pi^*$ of free –OH groups of PVA, depending on electronic spatial configuration within its molecules [38]. PEG is emissive (at ~ 380 nm) under the specific conditions of forming clusters of its chains (vesicles) [39]. CMC emissions ranged from near-infrared to blue, depending on the polarity of the solvent used [40].

ZnS has two emission peaks around 410 nm and 440 nm, which are attributed to a shallow state near its valance band due to zinc vacancies [41], and near its conduction band due to sulfur vacancies [42]. Compared to pure blend, Fig. 9a, the FL intensity is changed nonmonotonically with increasing the ZnS preparation temperature. The luminescence intensity reflects the density of states for a specific transition that is affected by several factors: carrier concentration, grain size, and transition energy. The FL intensity is increased for the polymer blends loaded with ZnS, as reported by Khan et al. [43]. For our samples, this occurred for the blends loaded with ZnS prepared at 300 and 400 °C. The enhanced luminescence is attributed to the ability of n-type ZnS to trap electrons and permit more holes to recombine

through the interface of PVA and ZnS. However, upon loading with ZnS prepared at 200 °C, the FL intensity decreased, most probably due to the high level of defects present in ZnS of low crystallinity, forming nonradiative centers and rendering the luminescence intensity [44]. The decrease in the FL intensity for the blend with ZnS at 500 °C may be caused by the increase in the grain size, thus decreasing the density of states [45], and/or the incorporation of O interstitially forming defects as indicated in x-ray part.

A Gaussian fitting was employed to decompose the emitted spectra for different samples, Fig. 9b and c. As noticed from the graph, the pure blend emitted UV, two violets, blue, and green colors. Upon loading PVA/CMC/PEG blends with ZnS prepared at 200, 300, 400, and 500 °C, the emitted colors became (two violets, blue, and green); (UV, two violets, and blue); (two UV, violet, blue, and green); and (UV, two violets, blue, green, and red) colors. The UV and violet colors are caused by the movement of electrons from near band emission (NBE) and/or excitonic transitions. The blue emission can be argued to be defect-related luminescence. The green sub-color resulted from the dopant or impurity atoms [46]. The red color is associated with the defects contained inside the blends, which are linked to the disorder in the blend matrix [47].

4 Conclusion

All ZnS samples used as nanofiller, prepared at 200, 300, 400, and 500 °C manifested a single phase of cubic zincblende structure ($F\bar{4}3m$). The crystallite size and cell parameters of the nanofiller were increased upon raising the annealing temperature, while the microstrain was reduced. A smooth surface with small pores nearly uniformly distributed was obtained for the pure polymer blend. The depth and size of the pores were increased upon loading with ZnS. The blend loaded with ZnS at 500 °C disclosed a heterogeneous surface with a larger pore size, cavity, and predominating. The absorption edge of the transmittance data exhibited a redshift with the largest value for the blend loaded with a ZnS sample prepared at 400 °C. The blends loaded with ZnS prepared at (200, 300 °C) and (300, 400 °C) have maximum shielding for UVB and UVA types, respectively. The direct and indirect optical energy gaps for the PVA/CMC/PEG blend are 5.52 and

5.12 eV, respectively, which are reduced as the blend is loaded with ZnS prepared at different temperatures. In the UV range, the refractive index gained the highest value for the blend loaded with ZnS prepared at 400 °C, while in the visible range, the refractive index (n) has the highest value with a ZnS sample prepared at 300 °C. The FL intensity of the pure blend was reduced as the nanofiller preparation temperature increased. The blends emitted UV, violet, blue, green, and red colors depending on the preparation temperature of the nanofillers. The NLO parameters attained their maximum values in the visible range as the blend was loaded with ZnS and prepared at 300 °C. The obtained blends can be employed in many optoelectronic, high-speed communications, and fast optical switching applications.

Author contributions

All authors have contributed, discussed the results and approved the final manuscript.

Funding

The authors are grateful to the Deanship of Scientific Research, King Saud University for funding through Vice Deanship of Scientific Research Chairs.

Data availability

The authors confirm that the data supporting the findings of this study are available within the article [and/or] its supplementary materials.

Declarations

Conflict of interest The authors declare that they have no conflict of interest.

References

1. T.H. AlAbdulaal, A. Almoadi, I.S. Yahia, H.Y. Zahra, M.S. Alqahtani, K.I. El Sayed Yousef, M.J. Hussein, F.A. Harraz, M.S. Al-Assiri, *Optik* **268**, 169741 (2022)
2. A.A. Menazea, N.S. Awwad, H.A. Ibrahim, M.K. Ahmed, *Radiat. Phys. Chem.* **177**, 109155 (2020)

3. A.A. Al-Muntaser, R.A. Pashameah, K. Sharma, E. Alzahrani, S.T. Hameed, M.A. Morsi, *Opt. Mater.* **132**, 112799 (2022)
4. A.M. El Sayed, S. Saber, *J. Phys. Chem. Solids* **163**, 110590 (2022)
5. M.I. Mohammed, *Opt. Mater.* **133**, 112916 (2022)
6. S.A. Issa, H.M. Zakaly, M. Pyshkina, M.Y. Mostafa, M. Rashad, T.S. Soliman, *Radiat. Phys. Chem.* **180**, 109281 (2021)
7. A.M. El-naggar, Z.K. Heiba, M.B. Mohamed, A.M. Kamal, G. Lakshminarayana, O.H. Abd-Elkader, *Opt. Mater.* **128**, 112379 (2022)
8. R.M. Ahmed, A.A. Ibrahim, E.A. El-Said, *Cta. Phys. Pol.* **137**(3), 317 (2020)
9. A.N. Al-hakimi, G.M. Asnag, F. Alminderej, I.A. Alhagri, S.M. Al-Hazmy, E.M. Abdallah, *Polym. Testing* **116**, 107794 (2022)
10. M.J. Tommalieh, *Radiat. Phys. Chem.* **179**, 109236 (2021)
11. M. Halajan, M.J. Torkamany, D. Dorrnian, *J. Phys. Chem. Solids* **75**(11), 1187 (2014)
12. K. Kannan, L. Guru Prasad, S. Agilan, N. Muthukumarasamy, *Optik* **170**, 10 (2018)
13. L. Dhatchinamurthy, P. Thirumoorthy, L. Arunraja, R. Subramanian, *J. Clust. Sci.* **30**, 827 (2019)
14. A. Tiwari, S.J. Dhoble, *RSC Adv.* **6**, 64400 (2016)
15. G.D.C. Pizarro, W. Alavia, K. González, H. Díaz, O.G. Marambio, R. Martin-Trasanco, J. Sánchez, D.P. Oyarzún, A. Neira-Carrillo, *Polymers* **14**(5), 945 (2022)
16. Z.K. Heiba, M.B. Mohamed, N.G. Imam, *J. Mol. Struct.* **1136**, 321 (2017)
17. A.M. El-naggar, Z.K. Heiba, M.B. Mohamed, A.M. Kamal, G. Lakshminarayana, M. AShar, *Optik* **258**, 168941 (2022)
18. A.M. El-naggar, Z.K. Heiba, A.M. Kamal, Y. Altowairqi, M.B. Mohamed, O.H. Abd-Elkader, A.A. Alhazime, *Opt. Mater.* **133**, 112923 (2022)
19. G. Rani, P.D. Sahare, *Appl Phys A.* **116**, 831 (2014)
20. L. Upadhyaya, J. Singh, V. Agarwal, A.C. Pandey, S.P. Verma, P. Das, R.P. Tewari, *J. Polym. Res.* **21**, 1 (2014)
21. R. Megha, Y.T. Ravikiran, S. Kotresh, S.C.V. Kumari, H.G.R. Prakash, S. Thomas, *Cellulose* **25**(2), 1147 (2018)
22. Y. Golitsyn, M. Pulst, M.H. Samiullah, K. Busse, J. Kressler, D. Reichert, *Polymer* **165**, 72 (2019)
23. J. Gao, X. Tang, Z. Chen, H. Ding, Y. Liu, X. Li, Y. Chen, *Polymer* **11**, 1503 (2019)
24. H.E. Assender, A.H. Windle, *Polymer* **39**, 4295 (1998)
25. R. Ricciardi, F. Auriemma, C. De Rosa, F. Laupretre, *Macromolecules* **37**(5), 51921 (2004)
26. A.M. Farah, F.T. Thema, E.D. Dikio, *Int. J. Electrochem. Sci.* **7**, 5069 (2012)
27. Q. Xia, X.J. Zhao, S.J. Chen, W.Z. Ma, J. Zhang, X.L. Wang, *Express Polym. Lett.* **4**(5), 284 (2010)
28. M.A. Morsi, A.H. Oraby, A.G. Elshahawy, R.M. Abd El-Hady, *J. Mater. Res. Technol.* **8**(6), 5996 (2019)
29. A. Chebil, B. Ben Doudou, C. Dridi, M. Dammak, *Mater. Sci. Eng. B* **243**, 125 (2019)
30. Y. Dai, Q. Tang, Z. Zhang, C. Yu, H. Li, L. Xu, S. Zhang, Z. Zou, *RSC Adv.* **8**, 38681 (2018)
31. H. Kafashan, M. Azizieh, H.N. Vatan, *J. Alloy. Comp.* **686**, 962 (2016)
32. M. Salah, M. Gad, M. Elkattan, Y.M. Sabry, *Opt. Commun.* **473**, 125933 (2020)
33. S. Ebraheem, A. El-Saied, *Mater. Sci. Appl.* **04**, 324 (2013)
34. G. N. Tiwari, T. Arvind, Shyam, *Handbook of Solar Energy, Theory, Analysis and Applications*, n.d., (2016)
35. K. Tanaka, *Thin Solid Film* **66**, 271 (1980)
36. F.A. Abdel-Wahab, M. Salah, H. Abdelmaksoud, *Mater. Chem. Phys.* **272**, 124989 (2021)
37. A.G. El-Shamy, *Prog. Org. Coat.* **150**, 105981 (2021)
38. D.M. Fernandes, A.A.W. Hechenleitner, S.M. Lima, L.H.C. Andrade, A.R.L. Caires, E.A.G. Pineda, *Mater. Chem. Phys.* **128**, 371 (2011)
39. C. Sun, X. Jiang, B. Li, S. Li, X.Z. Kong, *Sustain Chem. Eng.* **9**(14), 5166 (2021)
40. C. Wang, D.C. Popescu, C. Wu, J. Zhu, W. Macklin, Y. Wang, *J. Histochem. Cytochem.* **58**(7), 611 (2010)
41. P.V.B. Lakshmi, K.S. Raj, K. Ramachandran, *Cryst. Res. Technol.* **44**, 153 (2009)
42. S. Wageh, Z.S. Ling, X.X. Rong, *J. Cryst. Growth* **255**, 332 (2003)
43. M.M.R. Khan, S. Pal, M.M. Hoque, M.R. Alam, M. Younus, H. Kobayashi, *ACS Omega* **4**, 6144 (2019)
44. M.M.R. Khan, M. Akter, M.K. Amin, M. Younus, N. Chakraborty, *J. Polym. Environ.* **26**, 3371 (2018)
45. N. Akin, Y. Ozen, H.I. Efkere, M. Cakmak, S. Ozelcik, *Surf Interface Anal* **47**, 93 (2015)
46. S. Tao, S. Zhu, T. Feng, C. Xia, Y. Song, B. Yang, *Mater. Today Chem.* **6**, 13 (2017)
47. A. Manikandan, J.J. Vijaya, L.J. Kennedy, M. Bououdina, *J. Mol. Struct.* **1035**, 332 (2013)

Publisher's Note Springer Nature remains neutral with regard to jurisdictional claims in published maps and institutional affiliations.

Springer Nature or its licensor (e.g. a society or other partner) holds exclusive rights to this article under a publishing agreement with the author(s) or other rightsholder(s); author self-archiving of the accepted manuscript version of this article is solely governed by the terms of such publishing agreement and applicable law.